Supplement of Biogeosciences, 13, 903–912, 2016
http://www.biogeosciences.net/13/903/2016/
doi:10.5194/bg-13-903-2016-supplement

Supplement of

Calculations of automatic chamber flux measurements of methane and carbon dioxide using short time series of concentrations

N. Pirk et al.

Correspondence to: Norbert Pirk (norbert.pirk@nateko.lu.se)

Possible artifacts of temperature and relative humidity changes on calculated fluxes

Changes in temperature (T) and relative humidity (RH) of the monitored gas volume in the chamber headspace can affect the measurement process and thereby lead to artifacts in the calculated fluxes. To quantify the possible errors we simulated positive CH_4 fluxes and studied the artifacts of their chamber measurements due to changes in T and RH. Chamber parameters were chosen to resemble the ones described in the manuscript, i.e. a dimension of 0.6 m $\times$ 0.6 m $\times$ 0.3 m, and a closure time of 5 minutes. The initial dry CH_4 molar fraction was set to 1.8 ppm, while the final dry CH_4 molar fraction ranged from 1.9 to 4.4 ppm. The simulations imply linear increases in dry molar fraction from initial to final concentrations. Applying different T and RH values for the initial and final moment, and implying their linear change during the measurement, we analyzed wet CH_4 molar fractions as those obtained from the gas analyzer, and calculated the fluxes according to our usual routine. The range of fluxes corresponded to about 0.2 to 6 mg CH_4 m^{-2} h^{-1}. In the end those "measured" fluxes were compared with the "true" fluxes, and the error was expressed as the deviation in % from the true flux. Figure S1 shows these results for the following three scenarios, assuming initial conditions which are typical for our field sites during summertime.

Case 1: T constant at 10°C, RH changed from 75% to 100%.
In this situation two sources of error are combined:

- static dilution effect: the measured wet molar fractions are always lower than the corresponding dry molar fractions, so all fluxes are underestimated (in this case by about 0.9%);
- dynamic dilution effect: the water vapor dilution is increasing during the measurements, which appears as a small negative flux at a stable dry CH_4 molar fraction. This error is high in % expression at low fluxes, but becomes less important as fluxes increase.

In this case the error in fluxes is estimated to be $<$2% for fluxes $>$2 mg CH_4 m^{-2} h^{-1} and relatively increased for lower fluxes.

Case 2: T changed from 10°C to 11°C, RH changed from 75% to 100%.
This situation is more complicated:

- static dilution effect is the same as above;
- dynamic dilution effect is enhanced, as the same RH gives higher water content at higher temperature;
- T increase causes gas expansion, which is not accounted in our flux calculation routine.

Depending on what T value was used in the flux calculations, the cumulative error can be different. In fact, the error caused by neglecting gas expansion compensates the error caused by neglecting the dilution by water vapor to a large extend.

Case 3: T changed from 10°C to 12°C, RH changed from 75% to 100%.
Here, the artifacts are caused by the same factors as above, but both dynamic dilution and gas expansion are stronger. In this case the effect of gas expansion is overriding the effect of dilution for low fluxes.

In reality, there are many other measurement errors, especially at low flux magnitudes, that make a high precision of flux estimation practically unreachable. Our simulation shows that changes in air temperature and humidity are not outstanding among them. Note also, that these processes should mainly affect the flux estimate, but not the curvature of the concentration change. The curvature estimate would be affected only if the relative humidity and/or temperature changed in a time-dependent manner (e.g. increase first, then decrease again) during the closure time, so that such effects will be even smaller than the flux errors discussed above.

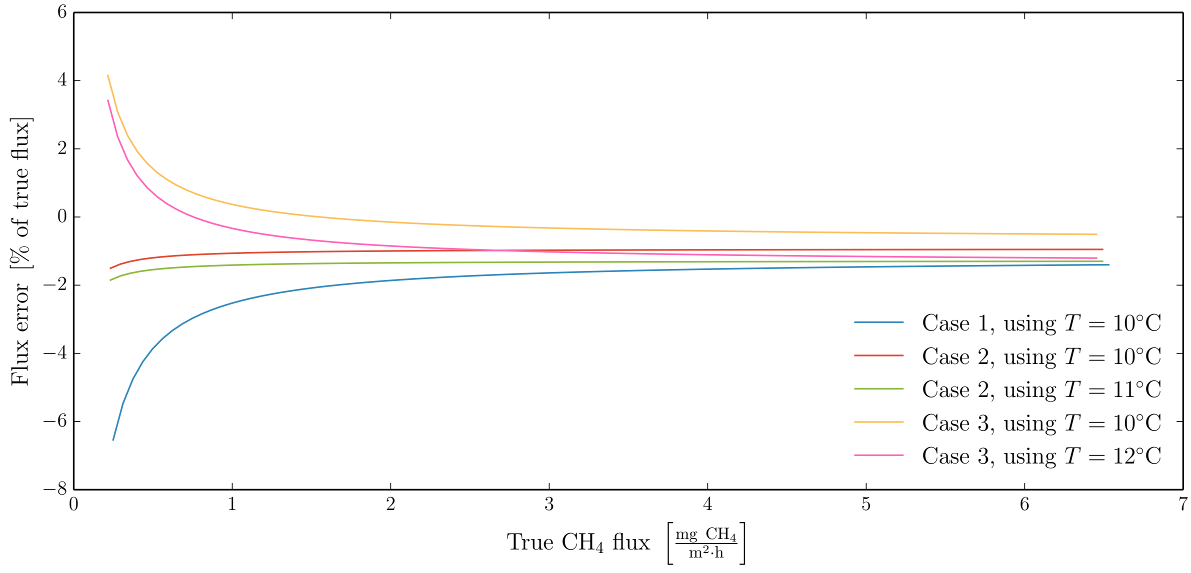

Figure S1. Simulated flux errors due to changing temperature and humidity in the chamber headspace.

Additional graphs

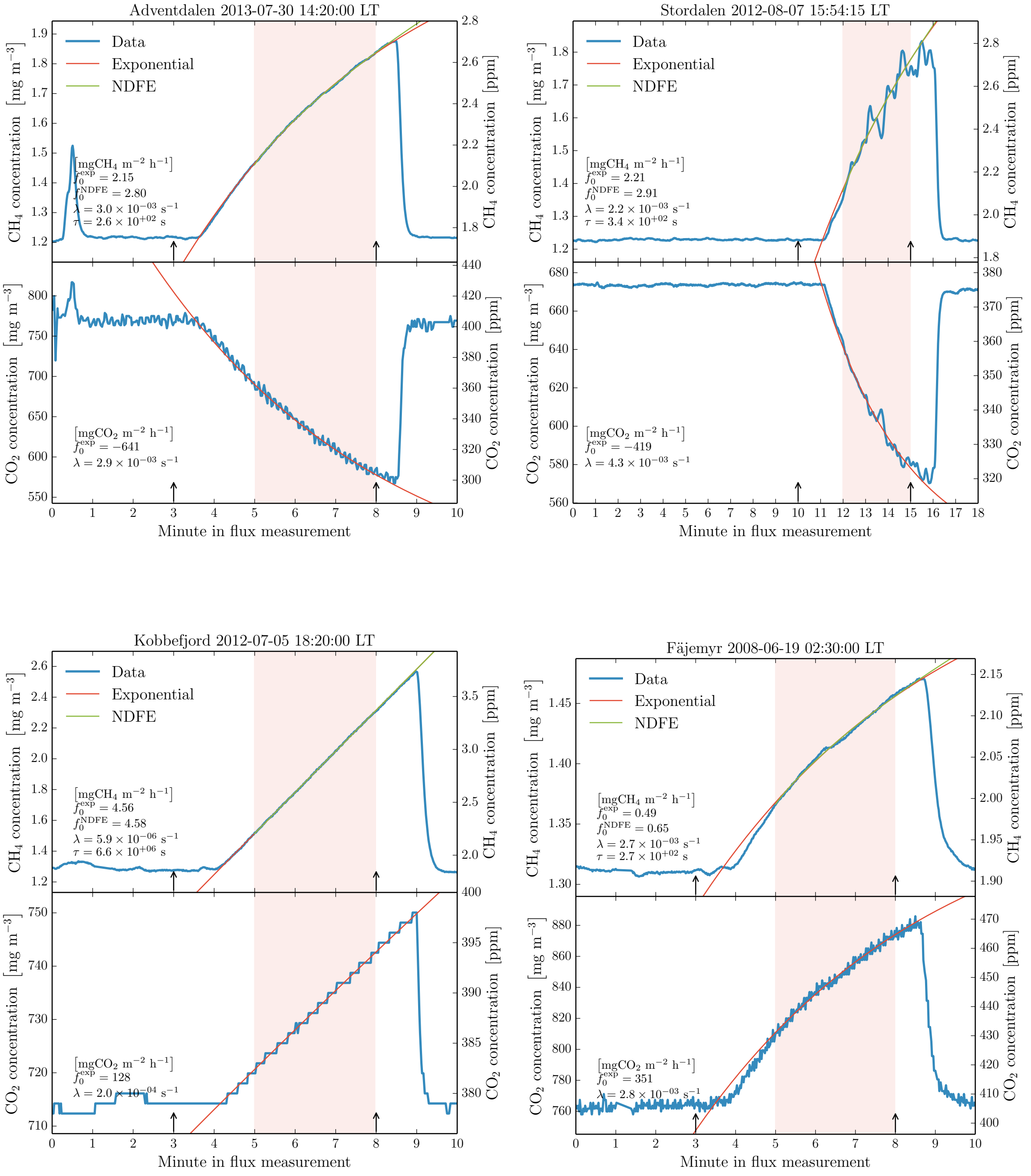

Figure S2. Flux measurement examples of $\mathrm{CH_4}$ and $\mathrm{CO_2}$ from Adventdalen (top, left), Stordalen (top, right), Kobbefjord (bottom, left) and Fäjemyr (bottom, right).

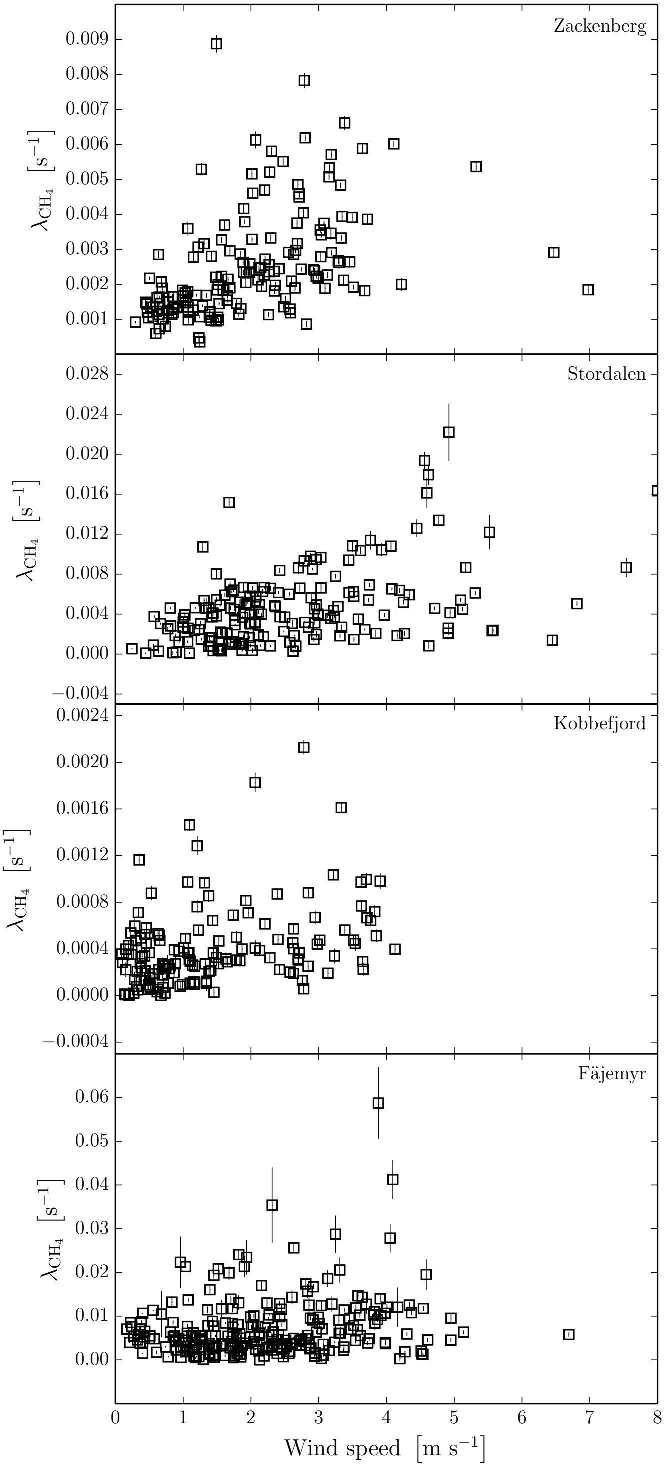

Figure S3. Curvature parameter λ_{CH_4} against wind speed for Zackenberg (chamber 6 between 24 June 2010 and 01 July 2010), Stordalen (chamber 2 between 01 August 2012 and 01 September 2012), Kobbefjord (chamber 6 between 12 August 2012 and 22 August 2012), and Fäjemyr (chamber 6 between 30 July 2008 and 15 August 2008).

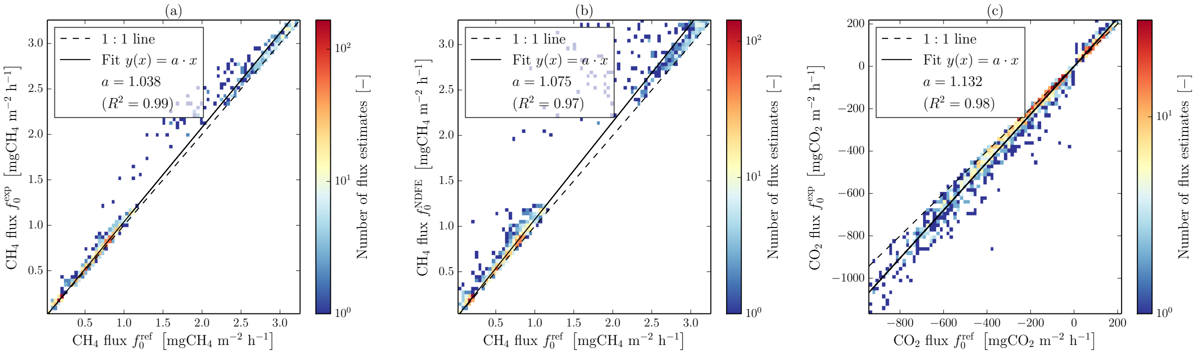

Figure S4. Histograms of flux estimates against reference flux for all chambers of Adventdalen. (a) CH$_4$, exponential. (b) CH$_4$, NDFE. (c) CO$_2$, exponential.

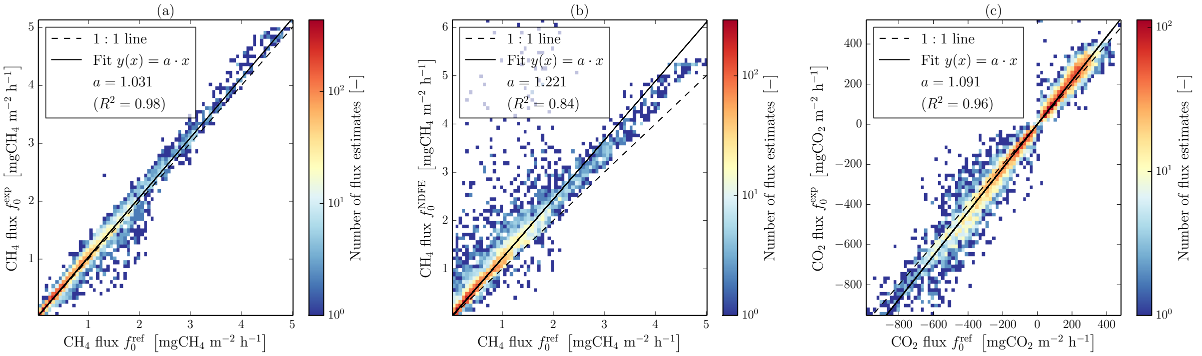

Figure S5. Histograms of flux estimates against reference flux for all chambers of Zackenberg. (a) CH$_4$, exponential. (b) CH$_4$, NDFE. (c) CO$_2$, exponential.

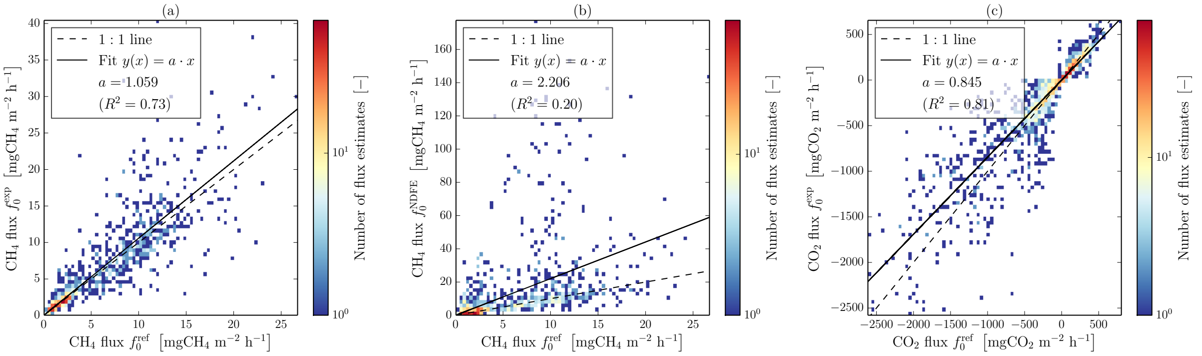

Figure S6. Histograms of flux estimates against reference flux for all chambers of Stordalen. (a) CH$_4$, exponential. (b) CH$_4$, NDFE. (c) CO$_2$, exponential.

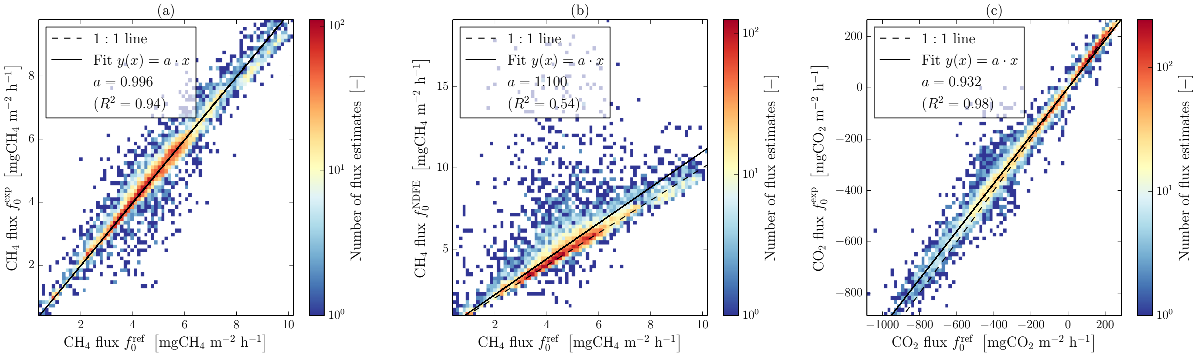

Figure S7. Histograms of flux estimates against reference flux for all chambers of Kobbefjord. (a) CH$_4$, exponential. (b) CH$_4$, NDFE. (c) CO$_2$, exponential.

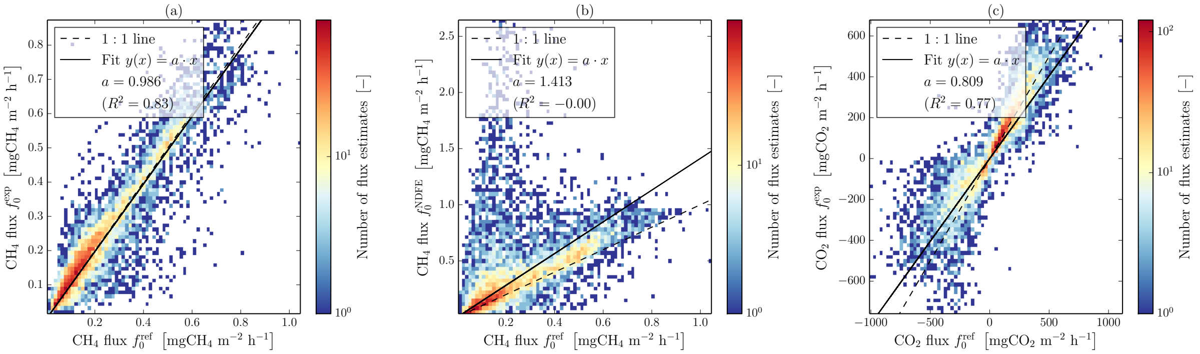

Figure S8. Histograms of flux estimates against reference flux for all chambers of Fäjemyr. (a) CH$_4$, exponential. (b) CH$_4$, NDFE. (c) CO$_2$, exponential.

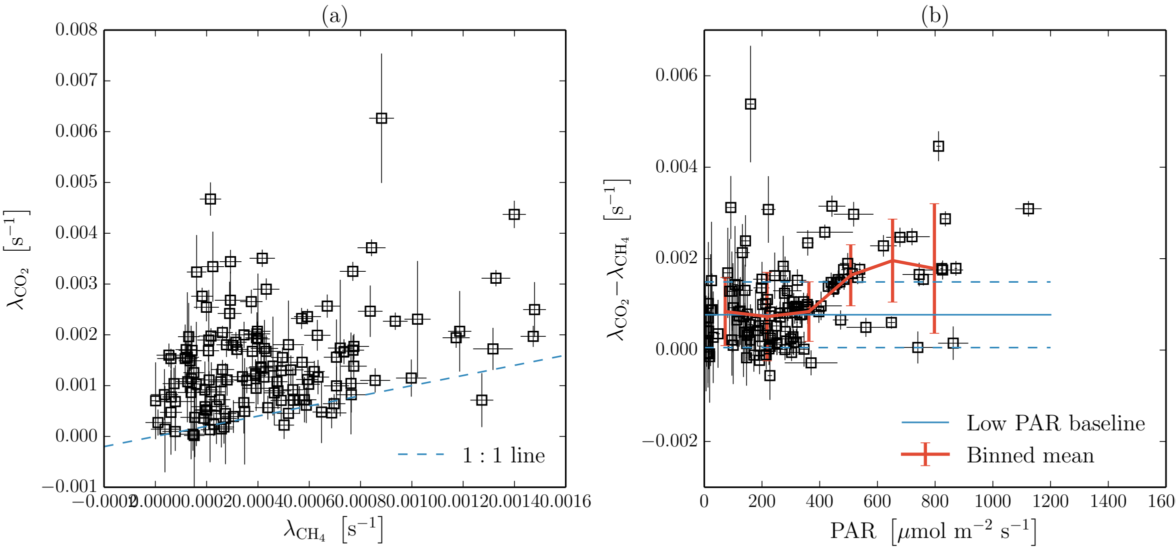

Figure S9. Curvature correlation (a), and curvature difference against PAR (b) of data from chamber 2 at Adventdalen. Error bars indicate standard errors as calculated by the least-squares fit.

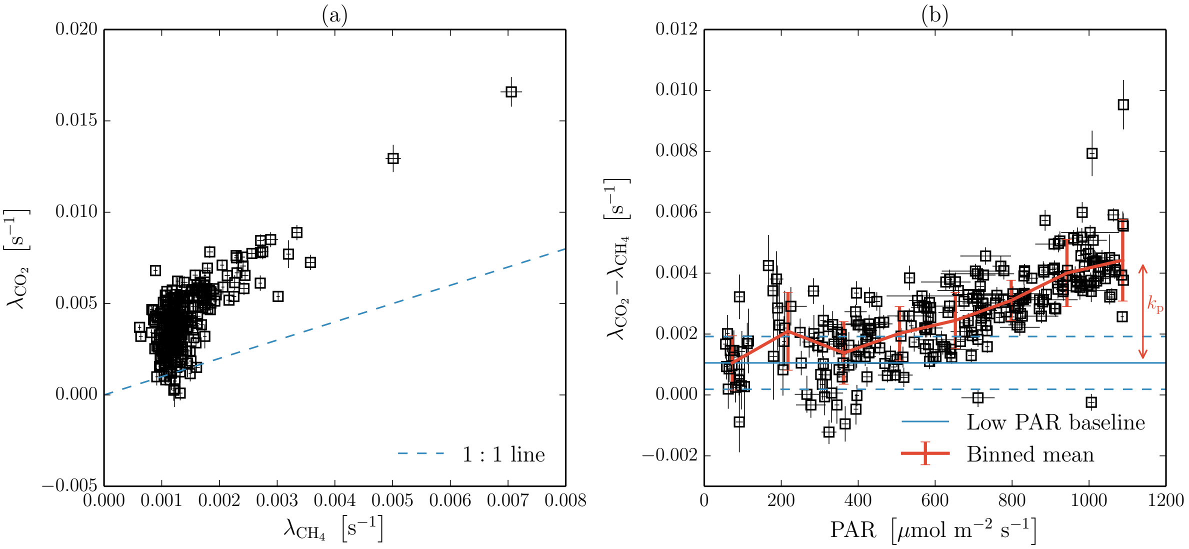

Figure S10. Curvature correlation (a), and curvature difference against PAR (b) of data from chamber 1 at Zackenberg. Error bars indicate standard errors as calculated by the least-squares fit.

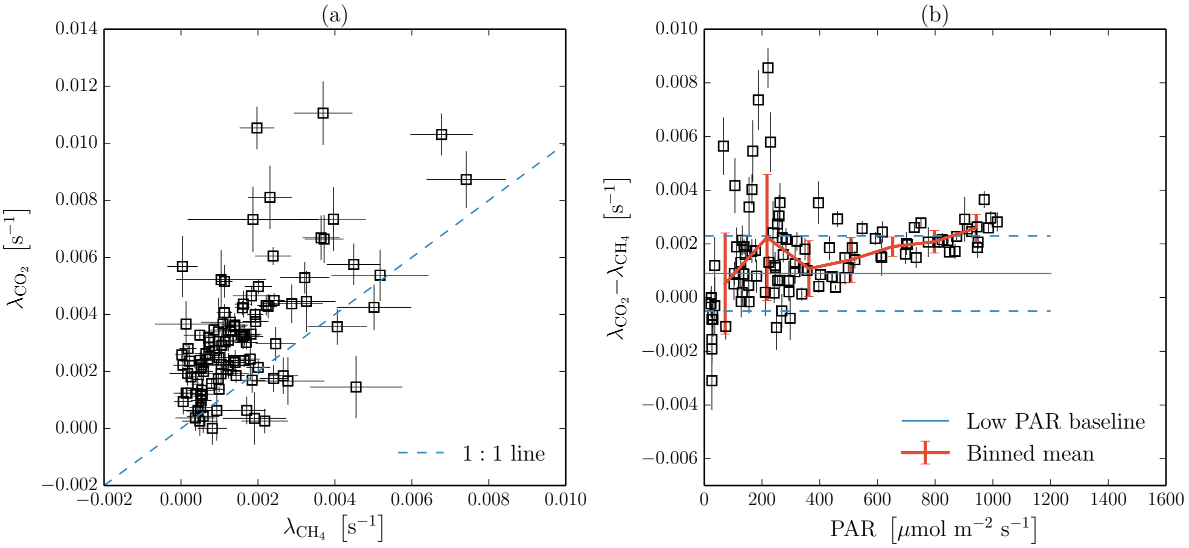

Figure S11. Curvature correlation (a), and curvature difference against PAR (b) of data from chamber 6 at Sordalen. Error bars indicate standard errors as calculated by the least-squares fit.

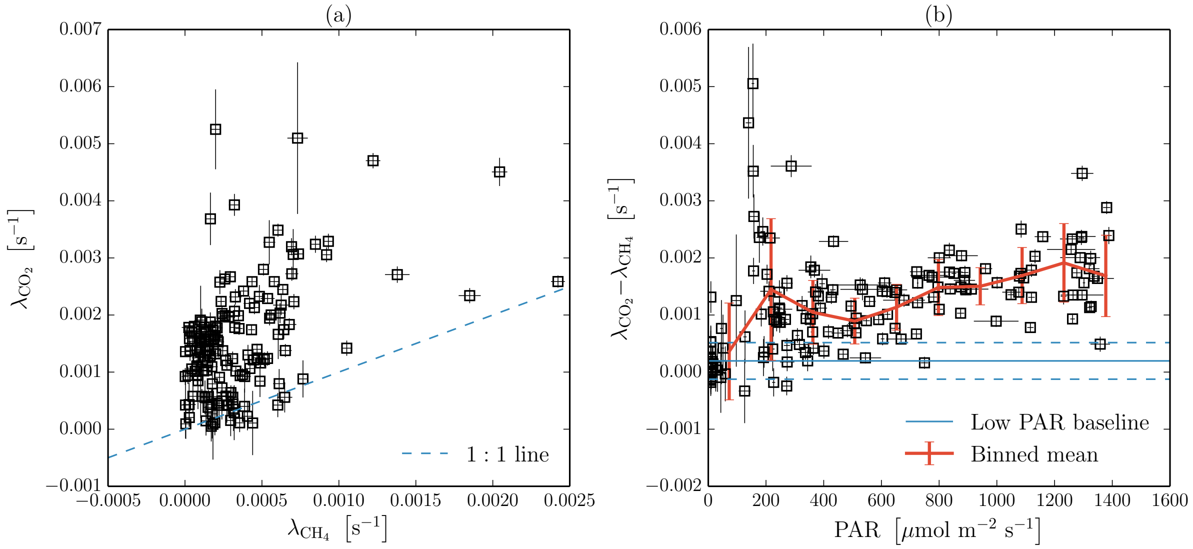

Figure S12. Curvature correlation (a), and curvature difference against PAR (b) of data from chamber 2 at Kobbefjord. Error bars indicate standard errors as calculated by the least-squares fit.

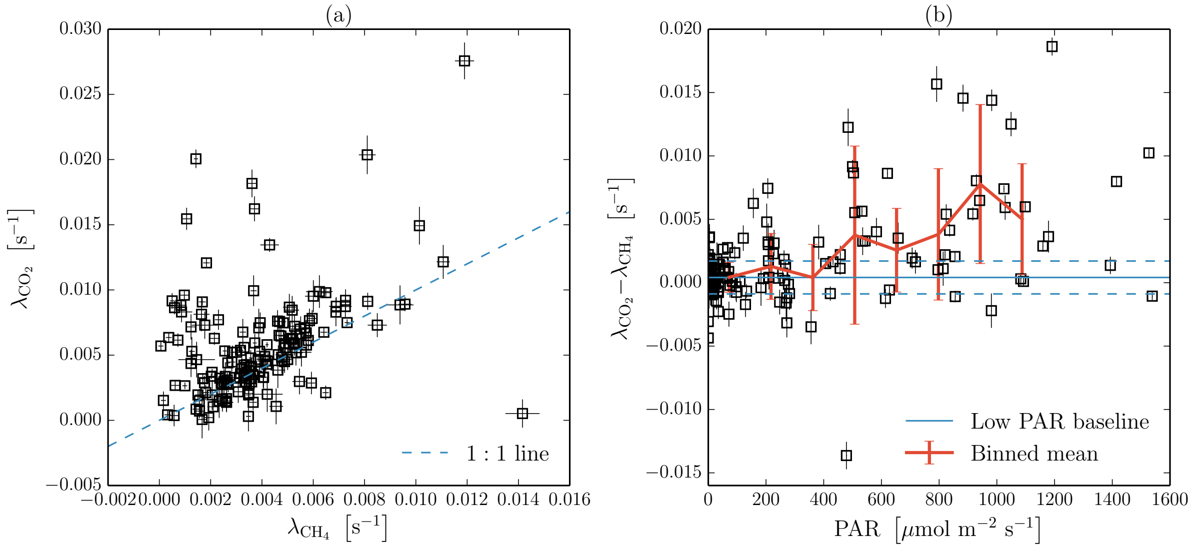

Figure S13. Curvature correlation (a), and curvature difference against PAR (b) of data from chamber 4 at Fäjemyr. Error bars indicate standard errors as calculated by the least-squares fit.